Likely Counter Point Bars in Coarse-grained Meandering Fluvial Deposits in the Brushy Basin Member of the Jurassic Morrison Formation

---

A Thesis

Presented to

the Faculty of the Department of Earth and Atmospheric Sciences

University of Houston

In Partial Fulfillment

of the Requirements for the Degree

Masters of Science

By:

Petter Dischington

May 2013

Likely counter point bars in coarse-grained meandering fluvial deposits in the Brushy Basin Member of the Jurassic Morrison Formation

_____

Petter Dischington

APPROVED:

_____

Dr. Janok P. Bhattacharya, Advisor

_____

Dr. William Dupré, Committee Member

_____

Dr. Brian Willis, Committee Member

_____

Dean, College of

Natural Sciences and Mathematics

Likely Counter Point Bars in Coarse-grained Meandering Fluvial Deposits in the Brushy Basin Member of the Jurassic Morrison Formation

---

An Abstract of a Thesis

Presented to

the Faculty of the Department of Earth and Atmospheric Sciences

University of Houston

In Partial Fulfillment

of the Requirements for the Degree

Masters of Science

By:

Petter Dischington

May 2013

Abstract

Fluvial deposits in the Tithonian Brushy Basin Member of the Morrison Formation were studied in order to create a facies architectural diagram and reconstruction of a fluvial system exposed in outcrop. This study provides an opportunity to study a coarse-grained meandering fluvial system, and provides one of the first descriptions of an ancient counter point bar in outcrop. Eleven measured sections across a 300m long outcrop were correlated on a photomosaic, creating bedding diagrams showing facies architecture and grain-size variations. The main channel facies shows a fining up succession from pebble to medium-grained sandstone, overlain by the fine sandstone and siltstone of the upper point bar. Four main facies were described, including a silty, mud-rich floodplain facies, a sandy thin laterally continuous facies showing convoluted bedding interpreted as overbank splays, a sandy, trough-cross-stratified channel fill facies and a silty, mud-rich counter point bar/ flood drape/ abandoned channel fill facies. Channel properties were assessed using the cross-sectional area of the channel and bedforms to discharge correlation. The channel was assessed to be 25.2m wide with an average channel depth of 5.6m. A flow discharge averaging 55 m^3/s was calculated by using the law of the wall to find the average flow velocity of water through multiple rectangles covering the channel cross-section. Initial results show the main outcrop to represent a single meander loop initially expanding as the fluvial channel flowed north, then

changing into eastward translation followed by further expansion. The deposits from the eastward translation of the fluvial channel show an eastward paleocurrent, concave bar deposits in the distal end of the meanderscrolls and are rich in silt- and mudstone, forming non-tidal, inclined heterolithic stratification, indicating a likely counter point bar deposit. Counter point bars (CPBs) originate as a meander scroll migrates laterally and encounters an obstacle in the form of an erosion-resistant substrate, forcing it to begin longitudinal translation. Thus the CPB is always located on the distal end of the point bar, before the cutbank.

Table of Contents:

Introduction

Coarse-grained meandering fluvial systems and counter point bars are rarely described in the literature, especially in outcrop (Smith et al., 2009). This study will describe a 300 meter-wide outcrop in the Jurassic Brushy Basin Member of the Morrison Formation that is thought to represent a coarse-grained meandering fluvial system, and evaluate the likelihood of inclined fine-grained deposits exposed in the outcrop being counter point bars.

Counter Point Bars

Counter point bars (CPBs) are described as a fine-grained, concave deposit on the distal end of a point bar (Makeske and Weerts, 2005). CPBs occur as a meandering river encounters an erosion-resistant substrate as it migrates laterally, and is forced to initiate longitudinal downstream migration. Such erosion-resistant substrates can be incised valley margins, oxbow lakes, abandoned channel fills, or older counter point bars (Smith et al., 2009; Makaske and Weerts, 2005). In the older literature, these deposits are described as concave-bench deposits, and were thought to only form where the fluvial channel bent in a hairpin tight curve, related to flow separation as well as eddy currents (Page and Nanson, 1982; Woodyer, 1985; Hickin, 1986; Hickin, 1979). Eddy-generated counter point bar deposition would generate an erosional scour on the base of the channel. CPB deposition can also initiate when stream power is very low, and barely exceeds the energy required for erosion (Nanson and Page, 1983). The term counter point bar was first used by Smith (1987b), describing a different kind of deposit where

deposition of coarser than point bar sand and gravel material is transported over the point bar in chutes, and deposited distally to the front of the point bar.

CPB deposition occurs from a variety of processes, including fluvial terrace deposits and tidally influenced fluvial deposits. They are predicted to have the greatest preservation potential if deposited in near coastal environments (Makaske and Weerts 2005). Thickness of fine-grained deposits compared to the total thickness of the channel appears to be the main differentiation between the two types of deposits (Makaske and Weerts, 2005). Some examples of inclined heterolithic stratification in Thomas et al. (1987), where clay-rich beds are superimposed to form a thicker clay-rich package, have later been interpreted to be CPB deposits (Smith et al., 2009). Corbeanu et al. (2004) describe inclined heterolithic stratification as a result of tidal influence in point bars, where the muddy parts of the deposit show burrows from marine influence.

Most previous studies of counter point bars are from modern rivers, as well as from cores of terrace deposits (Makaske and Weerts, 2005). Additionally, one study describes CPBs from high-resolution shallow seismic and core data of the Cretaceous McMurray Formation in Alberta (Smith et al., 2009). The above-mentioned study appears to be the only published study describing ancient CPBs.

Coarse-grained Meandering Fluvial Systems

Meandering fluvial systems are ordinarily thought of as fine-grained systems, and the suspended sediment load of all meandering rivers largely consists of clay and silt. Even rivers described as coarse bedload rivers typically have a suspended fine sediment

load of over 80% (Schumm, 1967). There are many studies of modern coarse-grained meandering fluvial systems, while descriptions of ancient coarse-grained meandering rivers are less common. Studies of deposits from Quaternary gravelly meandering rivers include Ori (1982) and Campbell and Hendry (1987). Kostic and Aigner (2007) used GPR to describe a coarse-grained deposit showing trough-shaped deposits interpreted to be braided rivers, comprising laterally accreting coarse-grained deposits interspersed with sand. The upper deposits are interpreted to be from meandering fluvial deposits. McGowen and Garner (1970) compared coarse-grained meandering fluvial deposits of the modern Colorado River in Texas and the Amite River in Louisiana, with Pleistocene deposits of the Colorado River and the Eocene Simsboro Formation in Texas. Modeling studies of coarse-grained meandering systems are fairly abundant, mainly due to the ease of scaling these systems from flume studies (Peakall et al. 2007, Braudrick et al. 2009, Pyrce and Ashmore 2005).

Regional Stratigraphy and Geologic Setting

The outcrop in this study was deposited within the Brushy Basin Member of the Morrison Formation, deposited during the Tithonian stage of the Jurassic. The Sevier orogeny commenced to the west and southwest of the area of deposition, and the rivers comprising the depositional system are flowing in a general east to northeast direction (Robinson and McCabe 1997).

Deposition occurred inland, with Lake Summerville farther to the northeast. Climate during the time of deposition is debated, with the Brushy Basin member traditionally thought to have been deposited in a dry, arid climate, but recent analysis of paleosols shows that the deposits could have originated in a wetter climate (VanDeVelde et al. 2006). Fielding et al. (2011) indicate the sparse, single-story channel deposits with poorly developed paleosols found in the Brushy Basin Member in the outcrop area could be partially due to a sub-humid to humid climate, in a dry climate one would expect laterally continuous, multi-story channel complexes.

The Morrison Formation is subdivided into three members in the study area: the Tidwell, Salt Wash, and Brushy Basin Members (fig. 1). High net-to-gross deposits, interpreted to be from braided fluvial systems, characterize the Salt Wash Member. The earliest Brushy Basin Member is also a sandy braided fluvial system that transitions into increasingly low net-to-gross deposits interpreted to be rapidly aggrading floodplain deposits with sparse meandering fluvial channels throughout. The formation is overlain by the Cedar Mountain Formation, which is truncated by a regional unconformity dividing the Jurassic and the Cretaceous, with the Dakota Formation immediately above (Robinson and McCabe 1997).

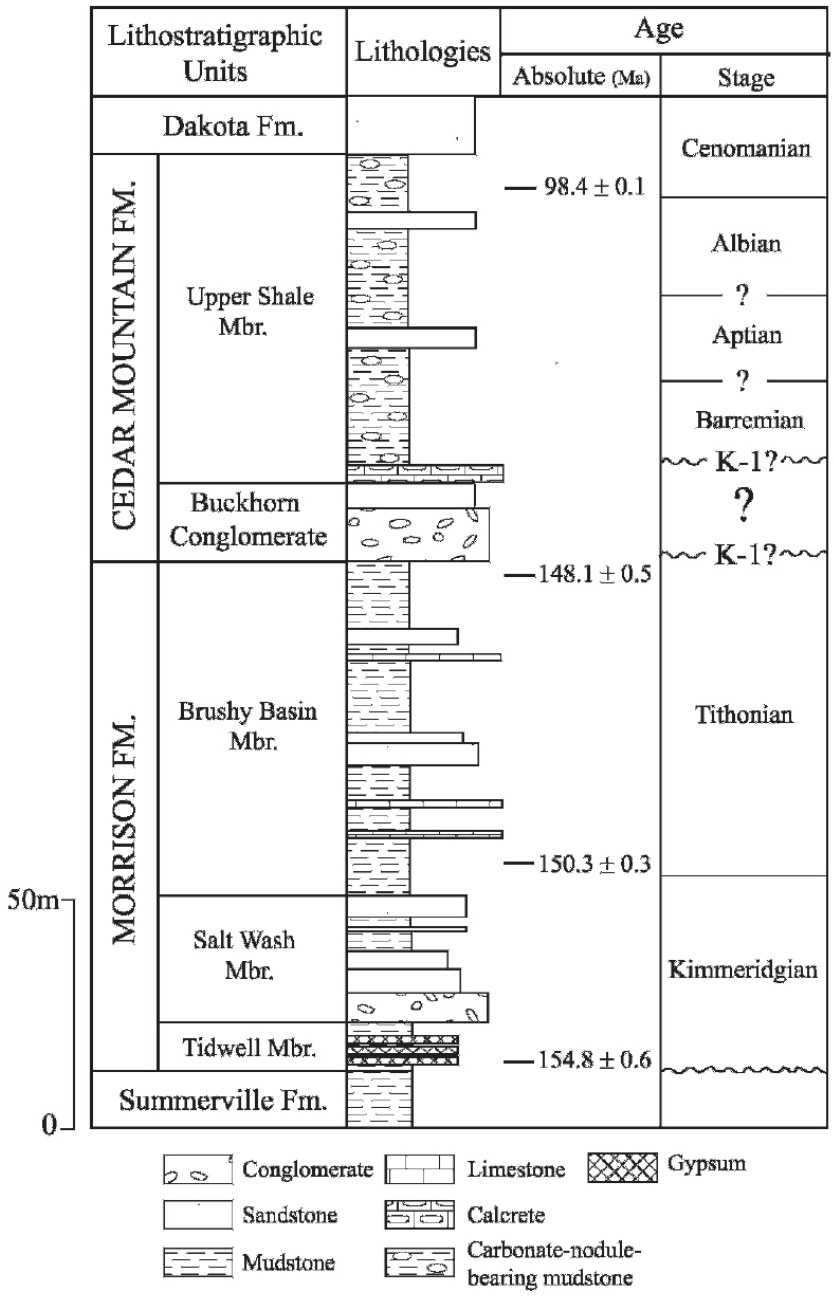

Figure 1. Section shows the Morrison Formation and surrounding stratigraphy in Central Utah. Notice the Brushy Basin Member superimposing the Salt Wash and Tidwell Members, while an erosional unconformity has eliminated the Buckhorn conglomerate at the studied location, indicating that the Brushy Basin member is likely superimposed by parts of the Upper Shale Member of the Cedar Mountain Formation and the Dakota Formation (from Roca and Nadon, 2007).

Brushy Basin rocks from the Kaiparowits Plateau and Dinosaur National Monument were dated using 40AR/39AR methods and show the rocks to be 153-145 ma. to the south and 135 ma. to the north (Kowallis, 1991). Brushy Basin rocks sampled near Hanksville were recently dated to 147 ma using U/Pb dating of zircons (Kowallis, 2007).

Study area

The study area is located 5 miles west of the town of Hanksville, in south central Utah (fig. 2). This area is on the eastern edge of the San Rafael Swell near Factory Butte. The studied outcrop has a length of 300 meters, and is oriented in an east-west orientation (fig. 3), with additional outcrop exposure several hundred meters to the east and to the west.

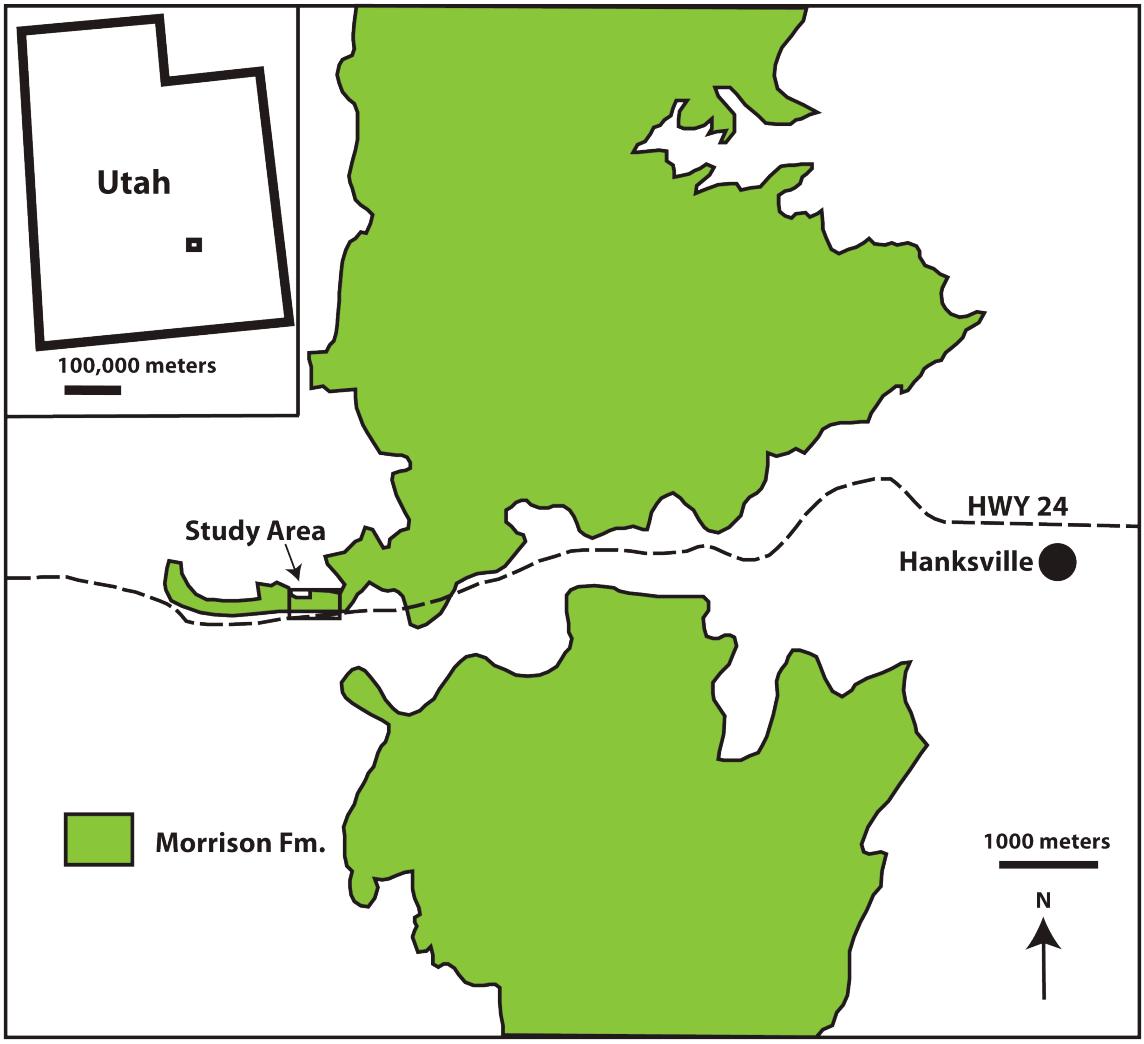

Figure 2. Map study area location in Utah with extent of Morrison Formation outcrops. Small box on large map shows location of the study area.

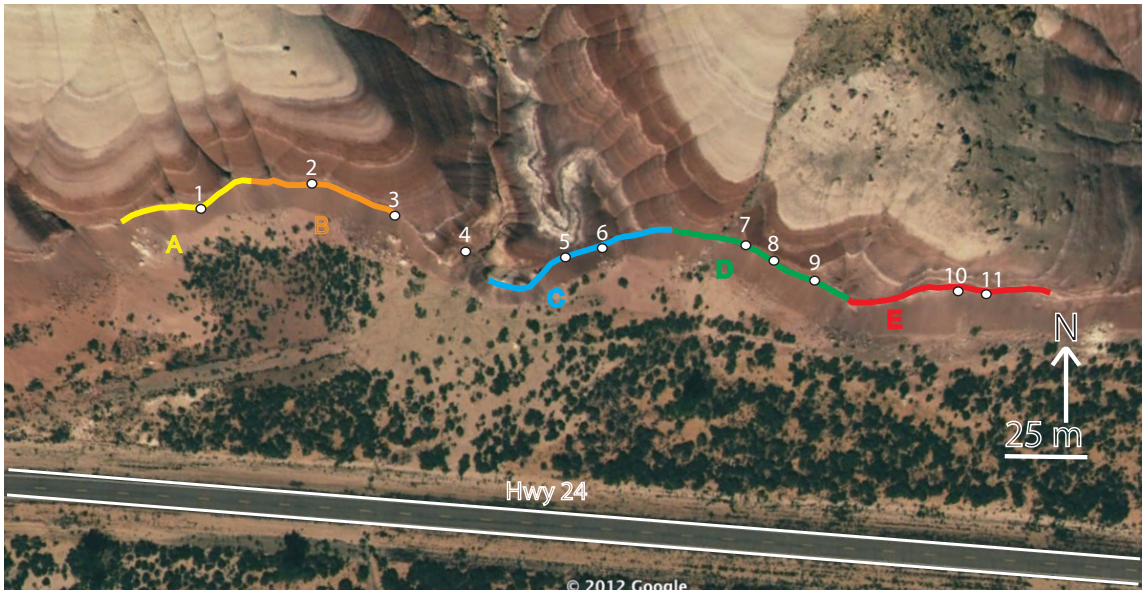

Figure 3. Satellite photo shows studied outcrop location. The thin lines (A-E) show the panel of outcrop in detail, and numbers indicate locations of measured sections (from Google Earth).

Methodology

A total of eleven measured sections (fig. 3) were acquired across the outcrop, with additional measured sections gathered to the east and west of the main outcrop. Measured sections included grain size, sedimentary structures, lithology, cross-set thickness, and paleocurrents. Vertical cliffs were measured while rapelling, and some exposures were trenched due to being covered. Clearing off clay residue on the outcrop surface was accomplished utilizing a spatula, stiff-haired brush and a flat-ended rock hammer. Sections were initially located by drawing them upon a photo of the outcrop surface and recording GPS location, then plotting and adjusting them in Google Earth to get accurate distances between them.

Detailed photos were taken of the whole outcrop using a Nikon D200 digital single-lens reflex camera with a Sigma 150-550mm telescope lens mounted on a tripod. Care was taken to ensure photos were taken perpendicular to the outcrop in order to minimize parallax. The photos were subsequently stitched together using Hugin and Adobe Photoshop software programs, resulting in a photomosaic encompassing 177 individual images.

Drafted measured sections were placed upon the photomosaic in order to create several bedding diagrams using Miall's hierarchy of surfaces (Miall, 1991) to show facies architectural elements, grain size variability within each depositional unit across the outcrop, as well as facies transitions. Paleocurrent measurements taken across the outcrop were plotted in rose diagrams for each half of the outcrop, with additional rose diagrams acquired over shorter expanses of outcrop in order to describe individual bar deposits. Using paleocurrent measurements, as well as facies architectural information, a 3-D reconstruction of the ancient fluvial system was completed in map view.

A comprehensive analysis of the fluvial system was performed. An average of channel depths was derived from channel deposit thicknesses in measured sections, and channel width was acquired from the photomosaic. The channel width was measured at an angle oblique to the flow direction, so trigonometric correction using the average paleocurrent measurement for the eastern outcrop was necessary. The channel cross-sectional area was estimated by using a standard equation for the area of a triangle:

$$A=(H*W)/2$$

In order to estimate the flow velocity and discharge of the river, multiple rectangles were drawn between a selected accretion surface and the water level in order for the rectangles to cover the channel cross section. The critical bed shear stress and the law of the wall were used to calculate the flow velocity for each rectangle, after which the flow velocities were multiplied with the area of each rectangle. The discharges for each rectangle were then added together and multiplied with 1.5 in order to account for the discharge of the entire channel cross-section.

Preserved channel fill was assumed to be total bar height, which represents 80% of total flow depth (Bridge, 2003), where these deposit thicknesses were determined from the measured sections and the photomosaic.

General Outcrop Description

The outcrop shows a major channel belt, overlain by floodplain mudstones and sandstones. The channel belt contains inclined heterolithic stratification throughout (figure 4), dipping east in the eastern part of the outcrop and west in the western part of the outcrop. Above the channel belt, the floodplain contains several thin, laterally continuous beds that are prevalent throughout the outcrop. The rest of the floodplain

deposits are dominated by purple to red siltstones and the channel deposits cut into these siltstones. The total apparent width of the outcropping channel belt deposit is ~275 meters, where the lateral extent is confirmed on the western outcrop by trenching, and is inferred on the eastern side of the outcrop due to the presence of a cut bank. The outcrop faces south and is oriented east to west, with cliff walls up to 40 meters vertical height. The bentonite-rich siltstone floodplain deposits have left a thick layer of sediment on the surface of the entire outcrop, and there is pervasive diagenesis in both the silt and sand grain-sized deposits, all contributing to limiting the visibility of sedimentary structures, especially within the channel deposits.

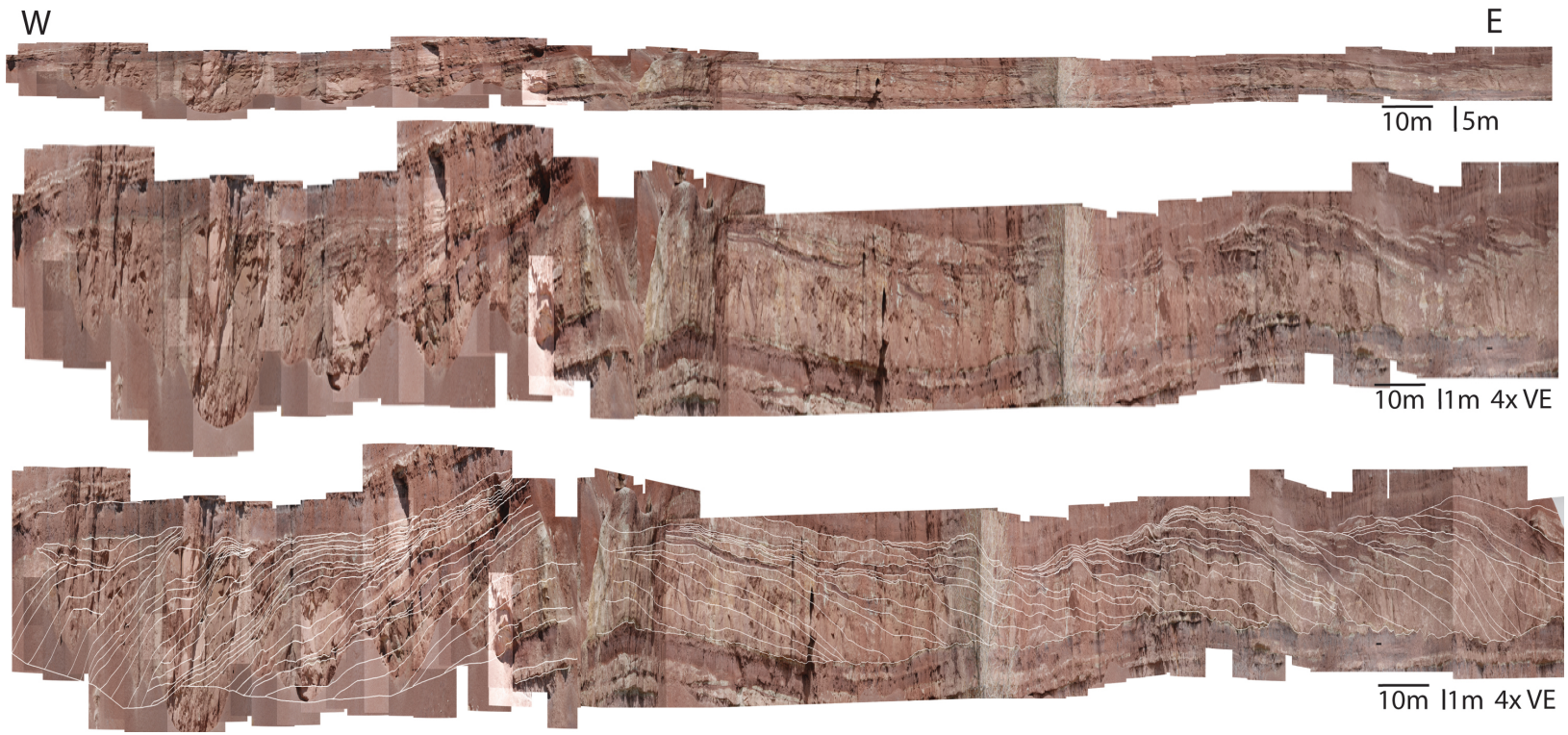

Figure 4. Photomosaic showing detailed image of studied outcrop, image has also been vertically exaggerated to show dipping surfaces better. Notice the western surfaces dipping west and the eastern surfaces dipping east, which is especially apparent in the third diagram which uses bedding diagrams to show bedding surfaces better.

Facies

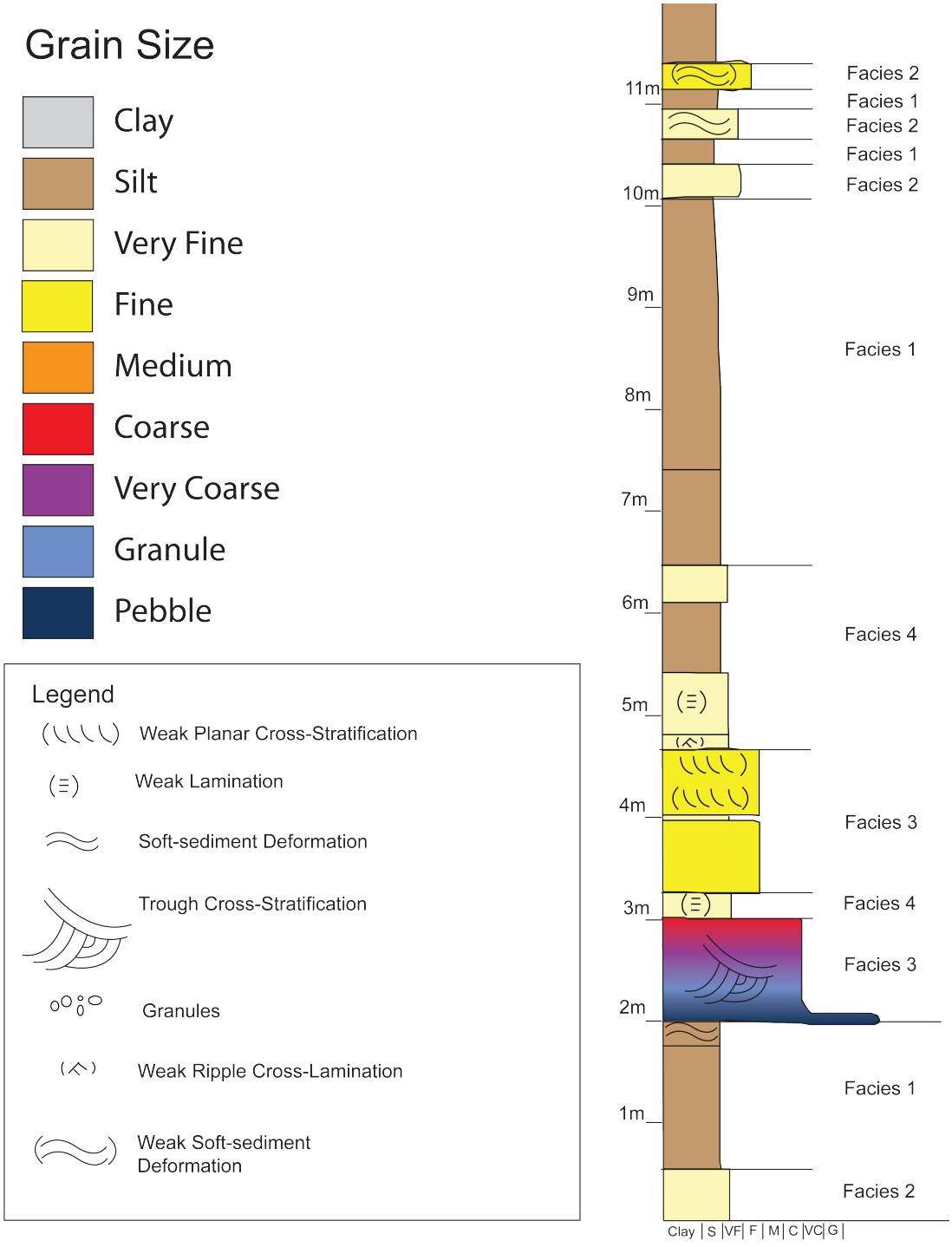

Figure 5. Diagram shows measured section consisting of facies 1-4.

Facies 1 comprises mudstone with a high concentration of silt and swelling clays and sparse amounts of very fine to fine sandstone (figs 5 and 6). The facies displays massive deposits with some weak indications of ripple and horizontal laminations, as well as occasional root structures. Units have thicknesses ranging up to tens of meters. The color of the facies varies from red to brown to bluish and greenish gray with mottling.

Interpretation:

Floodplain/floodbasin deposits are described by Bridge (2003) as silt and clay grain sizes with thin sandstone lenses, with abundance of bioturbation and fossils increasing in extent depending on the amount of time the area is flooded. The grain size distribution supports facies 1 being interpreted as floodplain deposits. The color and the root structures also indicate that this facies is a floodplain deposit.

Figure 6. Red to purple sandy siltstone, shows fissility.

Facies 2 comprises very fine- to fine-grained sandstone (figs. 5 and 7). The facies displays planar beds with some ripple cross-stratification, and deposits are mostly convoluted. Units have thickness from 0.15m-0.60m. The color of the facies is gray to yellowish tan.

Interpretation:

Bridge (2003) describes levee deposits as thin, elongate sand beds showing planar bedding and ripple cross stratification, and are often convoluted. Splay deposits are described as groups of these thin, elongate sand beds, with finer grain size silt/mudstone separating the deposits, and splay deposits cover larger areas than levee deposits. These deposits are thin and elongate with convoluted sedimentary

structures typical of levee and splay facies, and as exposed these units are hundreds to thousands of meters in lateral extent, fitting with the description of either levee or splay deposits.

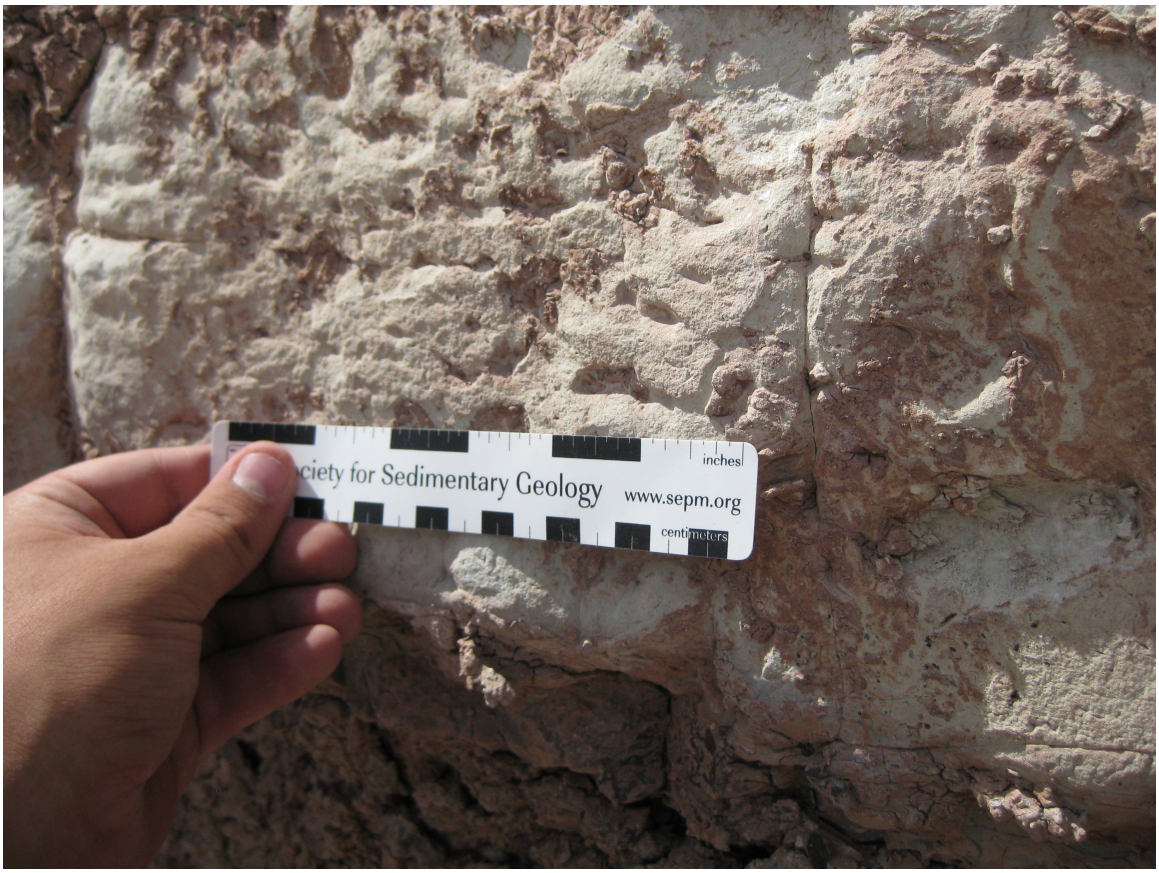

Figure 7. Thin, laterally continuous very fine to fine grained sandstone body showing soft-sediment deformation. Pervasive diagenesis obscures sedimentary structures.

Facies 3 comprises fine upper to very coarse sandstone, with coarser grain sizes up to pebbles (figs. 5, 8 and 9). The facies displays a fining up grain-size profile and dune-scale cross-stratification, with some weak ripple cross laminations, and

occasional lenses of coarse-grained granule to pebble-sized grains. Ripped-up mudclasts occur near bottom of units. Units have thicknesses from 2.5 to 5 meters.

Interpretation:

The coarse grain sizes and fining upwards profile indicates that facies 3 are interpreted as active channel fill deposits. This is additionally supported by the trough and ripple cross stratification indicating waning, unidirectional flows.

Figure 8. Graded deposits, fining up from sandy pebble conglomerate to coarse sandstone with granules.

Figure 9. Tan medium grain-sized to granule-sized trough cross-stratified conglomeratic sandstone.

Facies 4 comprises muddy siltstone to fine sandstone deposits rich in swelling clays (figs. 5 and 10). The facies displays a lack of sedimentary structures, with some weak ripple cross-stratification. Units have thicknesses of up to 2.5m. The color of the facies is reddish brown to purple.

Interpretation:

The deposits are interpreted as fine-grained fluvial deposits, either as flood drapes, counter point bar facies or abandoned channel fill.

Figure 10. Predominantly red to purple sandy siltstone, with a bed of tan very fine to fine sandstone. The siltstone is flaky with very weak indications of bedding as seen by color changes, while sedimentary structures in the sandstone body appears to be obscured.

Facies Diagram Description

The next section describes the lateral variability and distribution of the facies described above.

Facies Description West:

The western part of the diagram (fig. 11) shows fine-grained fluvial channel fill facies dipping westward and comprising up to 30% of the total thickness of the channel deposits. The channel facies cuts into the floodplain and levee facies. The channel facies are covered by floodplain facies, where one can also see levee facies.

The central to eastern part of the diagram is dominated by coarse-grained channel facies, with sparse fine-grained facies (~10%). Floodplain facies with thin, continuous levee facies unit superimposes the channel facies.

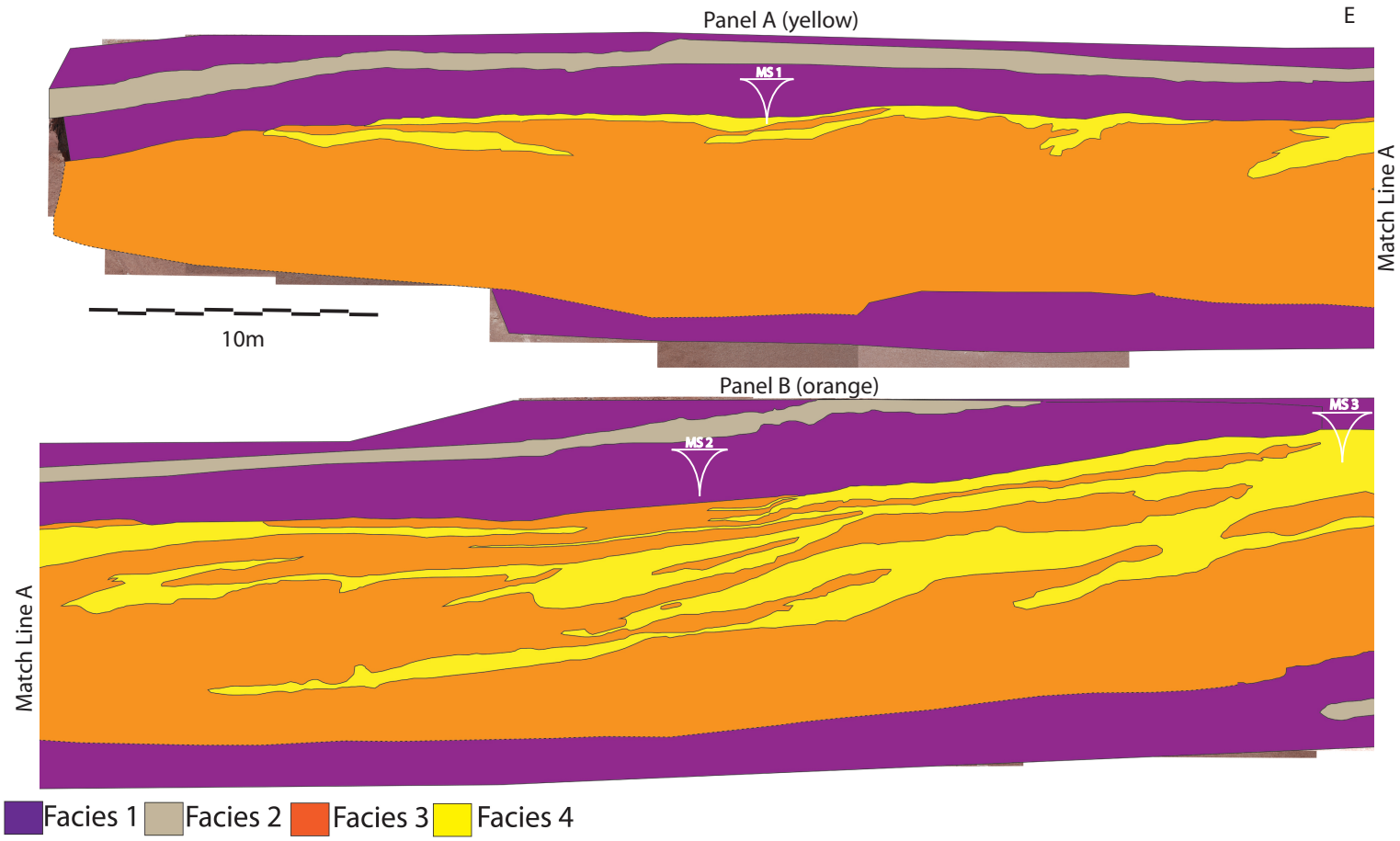

Figure 11. Panel A represents the westernmost part of the outcrop, and is characterized by a thick, fairly homogenous unit of facies 3, with a few thin slivers of facies 4. Facies 1 is found above and below the units of facies 3, with a thin elongate unit of facies 2 above facies 3. Panel B shows westward dipping units of facies 4 within facies 3. Location of panel A and B can be found in figure 3.

Facies Description East

The westernmost section of the diagram (panel C in figure 12) is dominated by coarse-grained channel facies, with a thin, eastward dipping unit of fine-grained channel deposits. The channel facies is cut into floodplain facies that has several elongate units of levee deposits.

The central to eastern part of the diagram shows coarse-grained channel facies with the upper ~20% of the channel deposits comprising fine-grained channel facies (panel D and E). The upper part of the channel deposits show distinct inclined heterolithic strata.

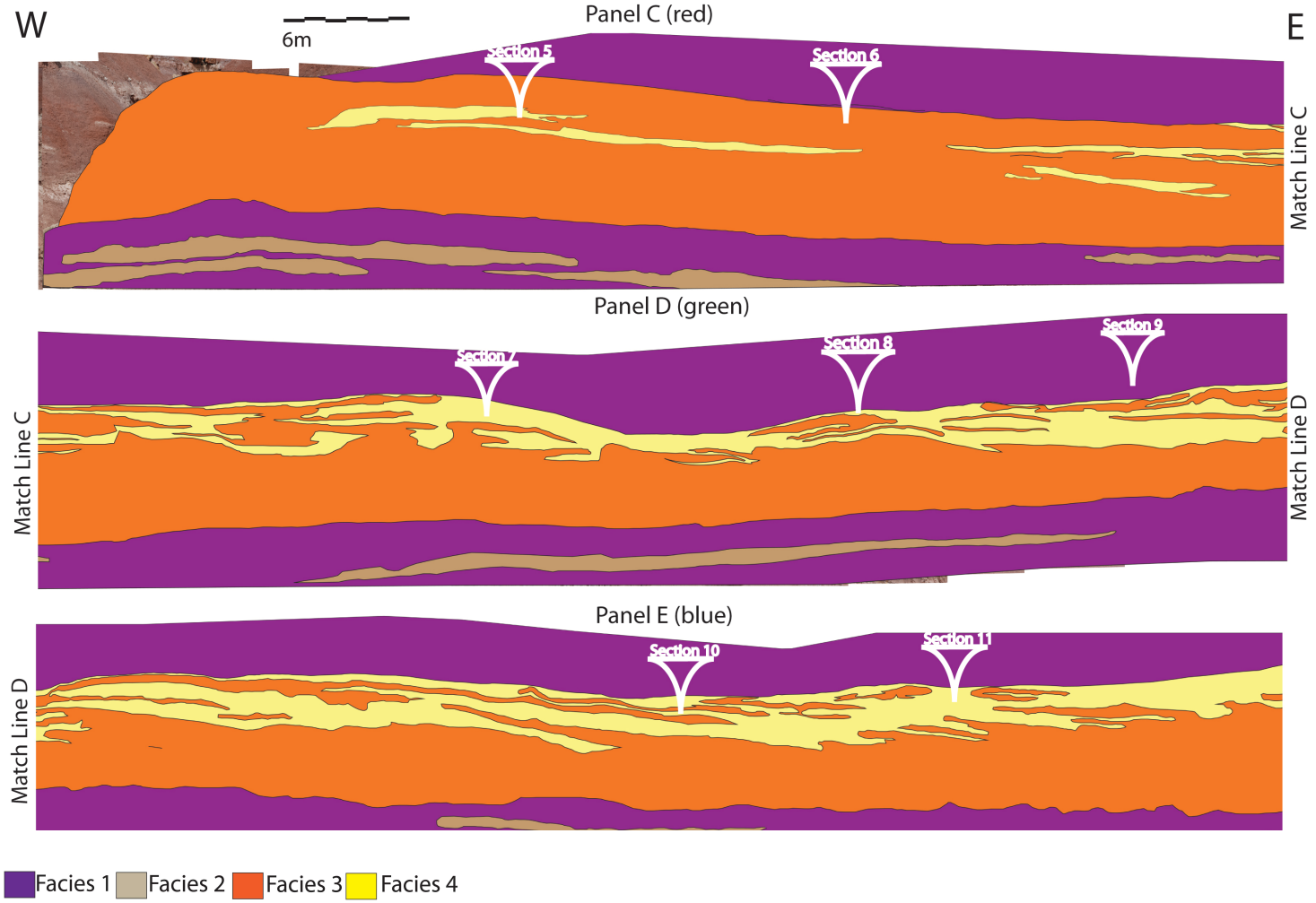

Figure 12. Panels C, D and E together make up the eastern part of the outcrop, with panel E being easternmost. Panel C shows only slivers of facies 4 within the larger unit of facies 3, and these units of facies 3 are dipping at a gentle angle. In panels D and E facies 4 forms a thicker unit superimposed on facies 3, with eastward dipping units of facies 4.

Hierarchy of Surfaces

Bedding diagrams were constructed using the hierarchy of Miall (1991). This hierarchy of surfaces ranks surfaces between fluvial channel architectural elements from 1 through 8 as follows:

0 – Lamination surface
1 – Set bounding surface
2 – Coset bounding surface
3 – Macroform
4 – Convex up macroform top
5 – Flat to concave up channel base
6 – Flat, regionally extensive
7 – Sequence boundary, flat, regionally extensive
8 – Regional disconformity

The surfaces used in construction of the bedding diagrams were mainly 3rd, 4th and 5th order surfaces, omitting the lower order surfaces. This allowed the description of bedforms in the bedding diagrams.

Bedding and Grain-size Variability Diagram

Overall

The diagrams show that the general dip direction in the eastern part of the outcrop is to the east, while in the western part of the outcrop the accretion surfaces are dipping to the west. Outcrop and panel geometry is located on the basemap (fig. 3), and they can also be seen as complete panels with rose diagrams in appendix 1.

West

The western part of the diagram generally shows accretion surfaces, with a presumed unit bar superimposed by convex up bedforms interpreted as a point bar (Segment V, figure 13). An erosional surface overlies the point bar deposit and is then followed by deposits interpreted to be from a chute channel.

There are five 4th order surfaces in the diagram, shown by the truncation of surfaces of 3rd order bar accretion surfaces (panel A).

Grain-size trends in segment I are generally very coarse (figure 13), while the upper portion of the deposits are characterized by fine- to silt-sized grains. Grain-size in the lower part of the deposits progressively fine and towards the western part of the outcrop, with the finer-grained, partially heterolithic upper half of the deposits becoming progressively more uniformly sandy in grain size distribution. The active channel deposits also thicken towards the west.

A grain-size shift from medium lower sandstone to fine upper sandstone signifies an erosional surface, and also transitions to steeper dipping accretion surfaces. West of this erosional surface (segment IV) the grain size is more uniform with the bottom being medium sandstone, fining to fine upper at the top, and the deposits are at their thickest.

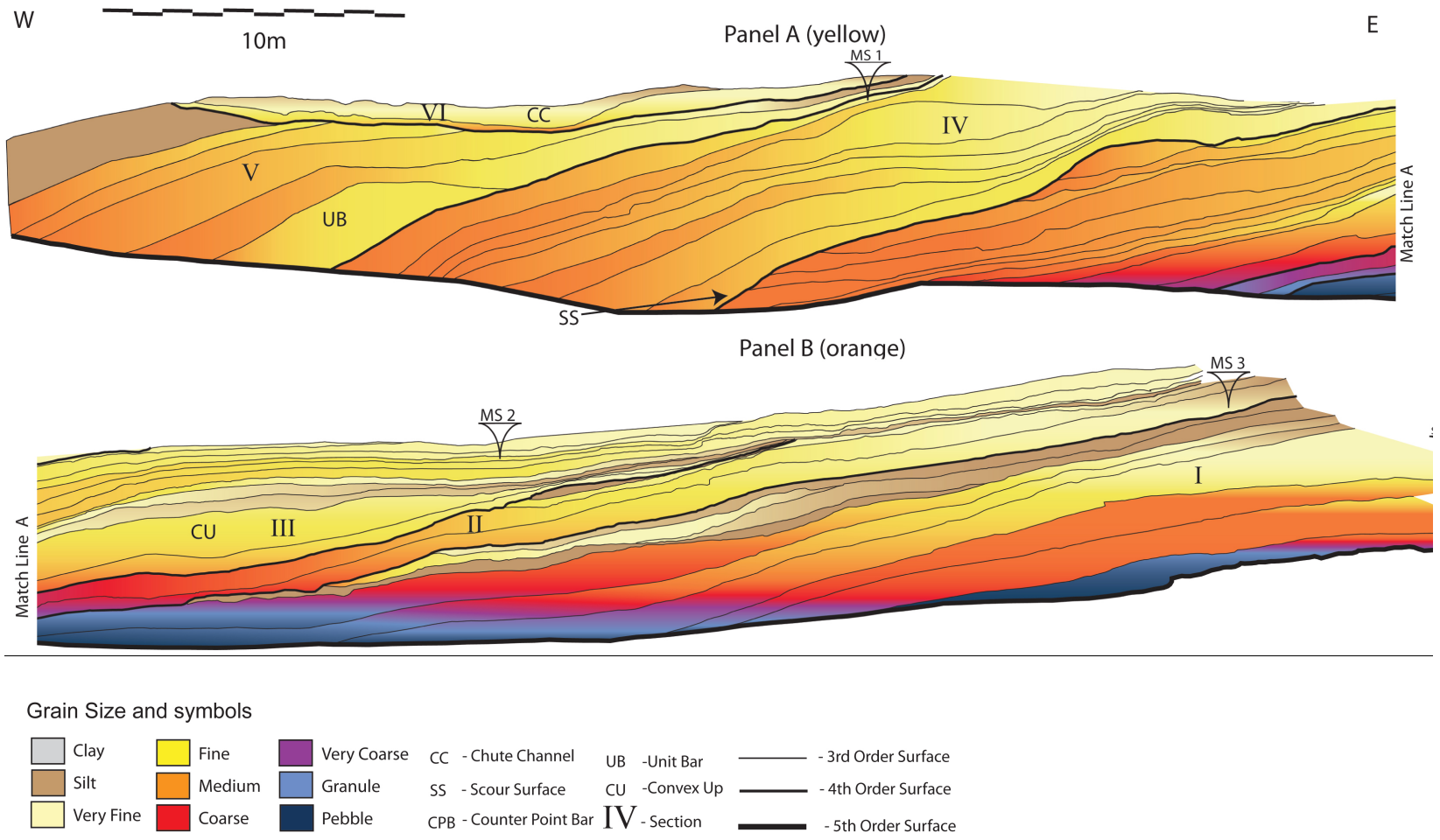

Figure 13. Figure shows grain size transition diagram of the western part of the outcrop, divided into two panels, A and B

East

The eastern part of the outcrop shows eastward dipping accretion surfaces, with the oldest, most westerly units being coarse (Segment I), with fine sandstone to granules (fig. 14 panel C), then transitioning laterally into finer grained, shallower dipping beds (fig. 14 panel C).

Between section 6 and section 7 the deposits transitions to coarser grain sizes than medium sand. Several of these depositional units also show convex up barforms. Grain sizes in the upper half of the diagram show a predominance of very fine sandstone and siltstone (fig. 14 panels C and D), with the deposits located at section 8 having up to 50% siltstone by thickness and can possible be counter point bar deposits.

Depositional units continue to dip at similar angles, while grain size appears to drop to finer grain sizes ranging from silt to coarse sand grain sizes (fig. 14 panel E) in the lower part of the deposit. The easternmost part of the outcrop (panel E) shows four 4^{th} order surfaces with fine-grained deposits above them (fig. 14 panel E), with the easternmost surface being clearly erosional, the subsequent surface shows onlap of depositional units, while the last two surfaces show slight erosion.

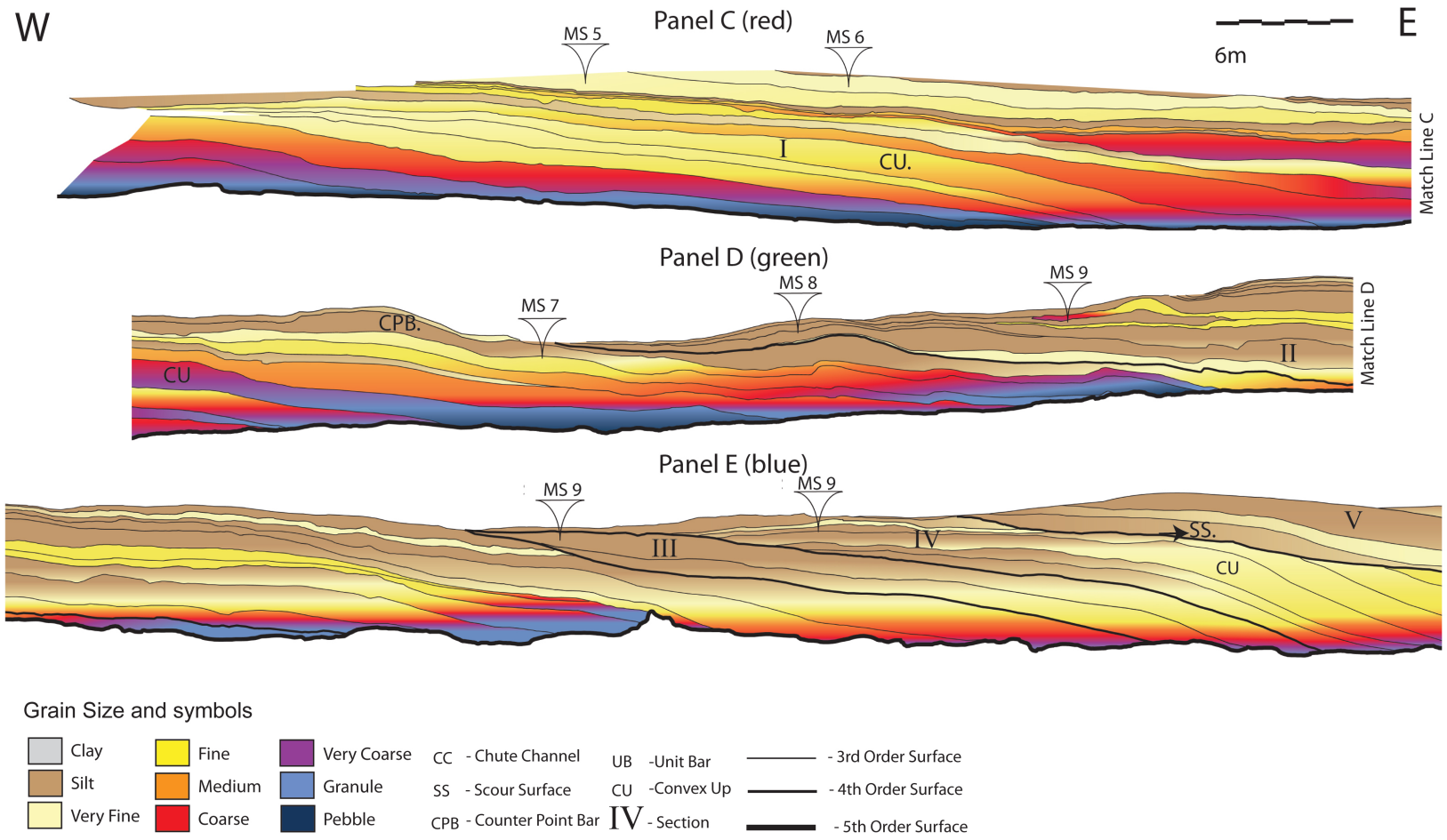

Figure 14. Shows the grain size transition diagram of the eastern part of the outcrop divided into three panels: C, D, and E.

Channel Reconstruction

The oldest deposits were found in the center of the outcrop, where the paleocurrent measurements are north to northwest (fig. 15 and 16), with the accretion surfaces in the channel body having a very gentle eastward apparent dip(segment I, figure 16). The outcrop is oriented obliquely to the paleocurrent direction, which probably accounts for the shallow apparent dip of the accretion surfaces (fig. 16). The composite point bar deposits are aggrading eastward as the meanderloop is expanding.

Further east in segment I (fig. 17, also shown by orange surface in figure 16) the paleocurrent measurements immediately to the east of the earliest deposits show paleocurrents going northeast (fig. 16), then transitioning to southeast. This transition in paleocurrent measurement direction is correlated to the presence of silt-rich deposits in the upper point bar, which is interpreted to likely being a counter point bar. The composite point bar deposits also thin towards the east, which is interpreted as the gradual transition from point bar to counter point bar deposits.

Segment I active channel fill deposits in the western part of the outcrop show paleocurrent measurements going southeast. This is interpreted to be the upstream reach of the meanderloop, and the deposits show a composite point bar aggrading westwards (fig. 18 east). The youngest part of the western segment I deposits are silt-rich and could be the distal end of an upstream counter point bar.

The fourth-order bounding surface between segments I and II in the eastern part of the outcrop (figure 19) shows a transition where the deposits above are

finer, and could have resulted from flooding (Bridge, 2003). Segment II deposits are generally fine-grained, with only a thin, coarse-grained base, and are interpreted to be counter point bars. The paleocurrents flow east to southeast, showing deviation indicative of counter point bars (Smith et al., 2009). In the western part of the outcrop segment II is a very thin deposit, and is coarser than segment I (figure 18). In the eastern part of the outcrop, segment III is a thin, fine-grained unit, and is interpreted to represent additional counter point bar deposits bounded by a minor flooding surface (figure 20, 21). In the western part of the outcrop, the point bar deposits aggrades and thickens westward, interpreted to result from expansion of the meanderloop with an additional increase in velocity (figure 18, 20).

The 4th-order surface bounding segment III and IV in the eastern part of the outcrop shows very minimal grain size change and erosion, and segment IV shows the point bar deposits thicken and expand. The western segment IV is bounded from segment III by a significant scour surface, with segment IV being finer-grained and steeper than segment III, and is interpreted as change in paleocurrents changing the trajectory of par migration (figure 18).

The eastern segment V is bounded by a scour surface, and is significantly more fine-grained than the deposits below, possibly due to channel abandonment (figure 21). In the western part of the outcrop segment V is a thinning point bar deposit and is bounded to the west by floodplain deposits representing the end of westward lateral expansion of the meanderloop. It is bounded above by a 4th order scour surface and the interpreted chute channel deposits of segment VI.

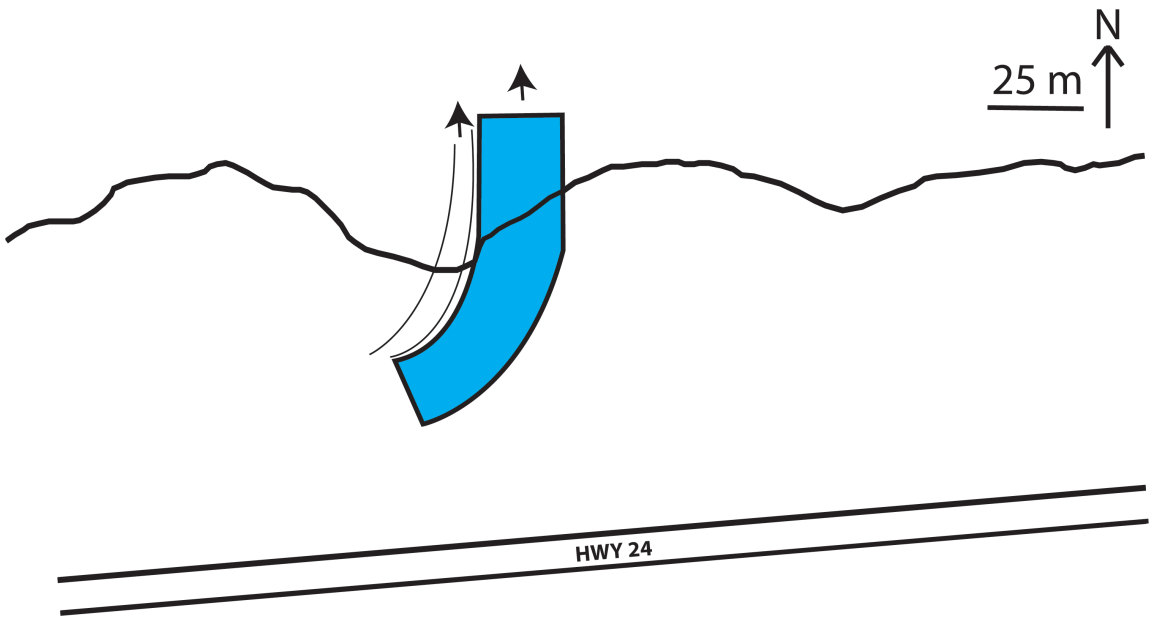

Figure 15 shows the oldest meandering fluvial deposits. Paleocurrent measurements dominantly show north to northwest flow direction, while the accretion surfaces of the point bar deposits are apparently dipping gently to the East. The reason for the gentle dip of these surfaces could be due to the high angle of the outcrop (map view outline of the outcrop shown by thin black line) to the paleo channel, giving a lower apparent dip than seen elsewhere in the outcrop. The meanderloop and its resulting deposits are shown to be expanding at this time.

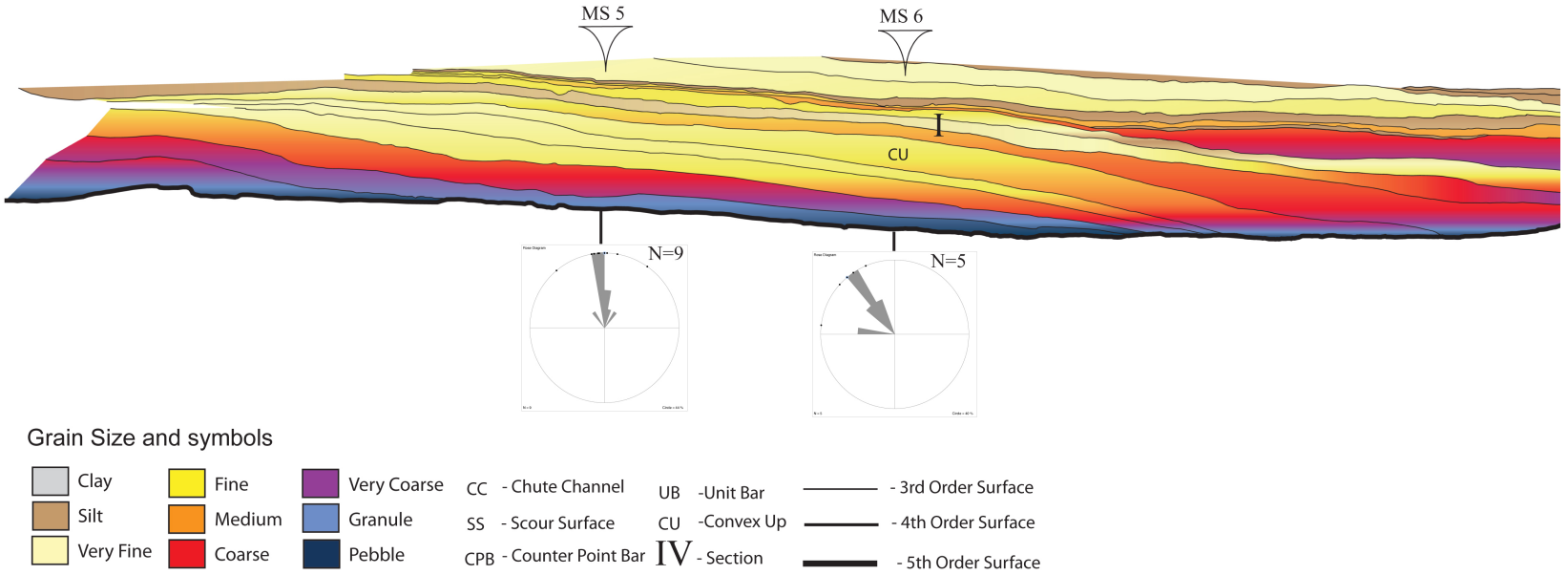

Figure 16. Bedding diagram showing the central part of the outcrop. Notice the paleocurrents (from crossbed dip direction) going north to northwest, while the accretion surfaces show an apparent dip to the East.

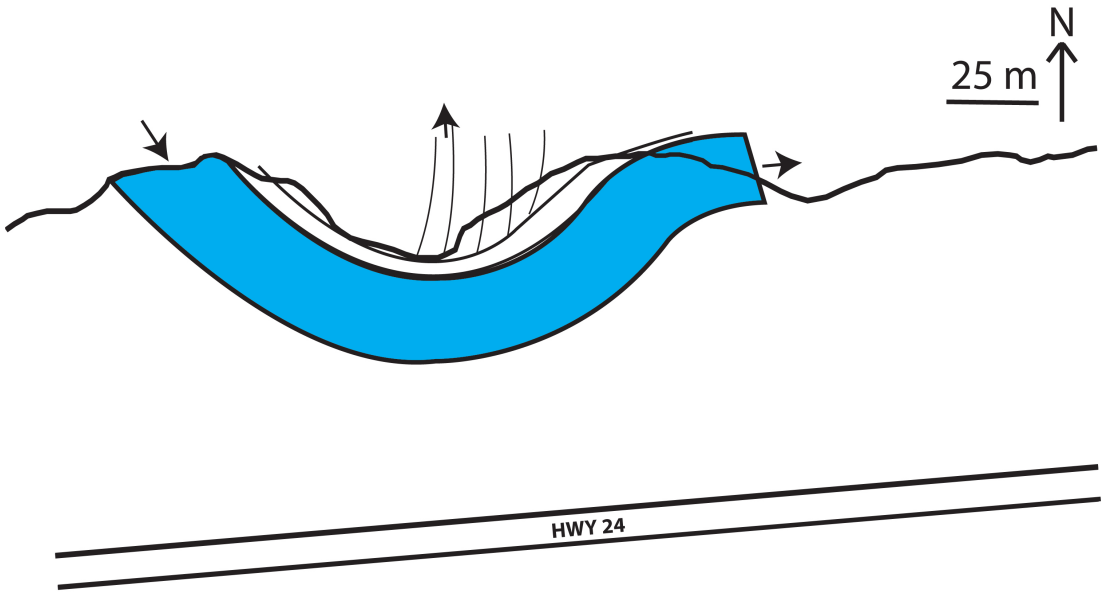

Figure 17 shows possible channel geometry at time 2. Notice the eastward paleocurrent at the easternmost end of the reconstruction. This is likely due to a counter point bar, as is also indicated by the thickening of the fine-grained deposits in the upper part of the channel deposits. At this time the meanderloop is showing eastward translation.

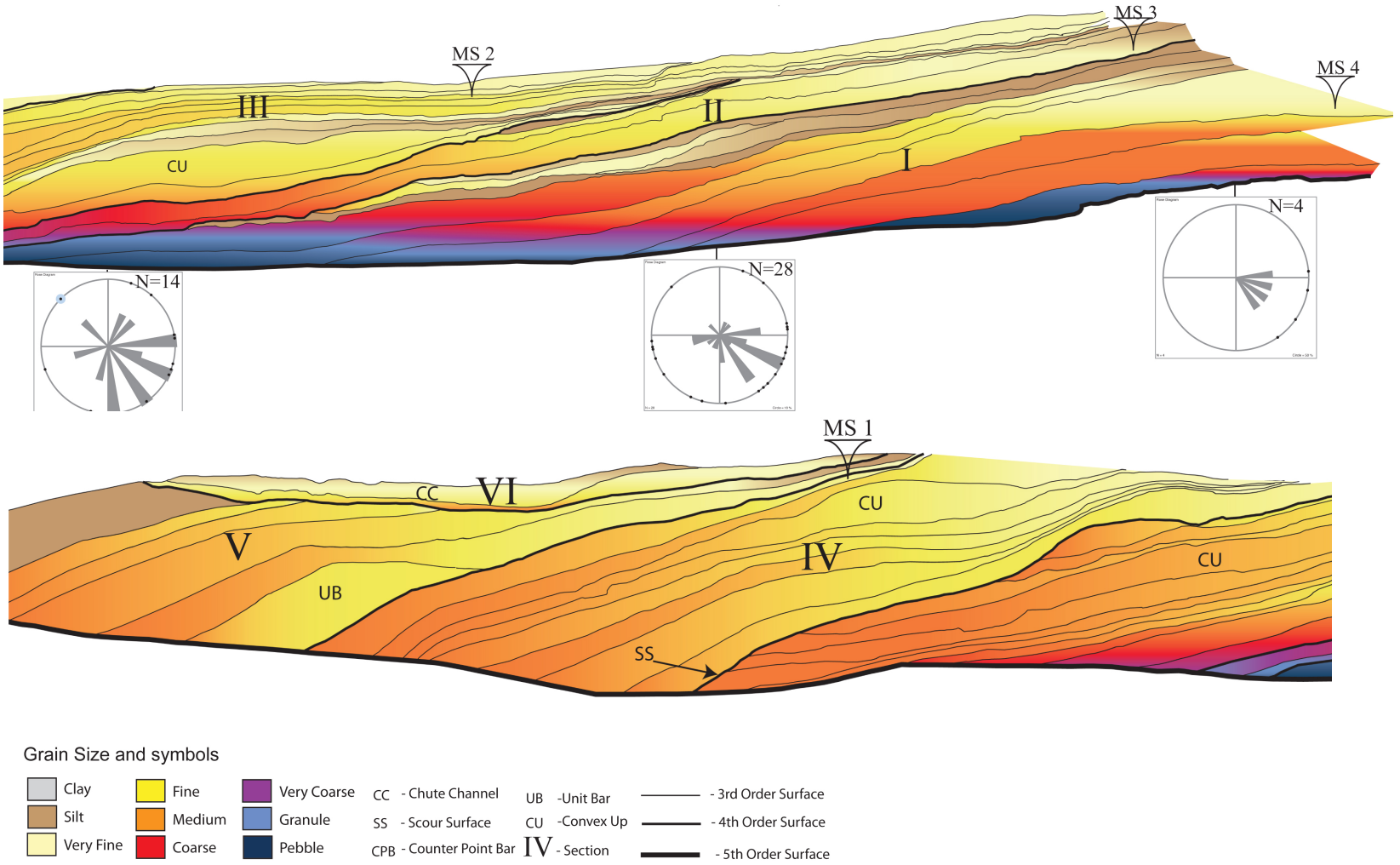

Figure 18. Bedding diagrams of the western side of the outcrop showing accretion surfaces dipping west, with rose diagrams showing paleocurrent measurements predominantly going southeast.

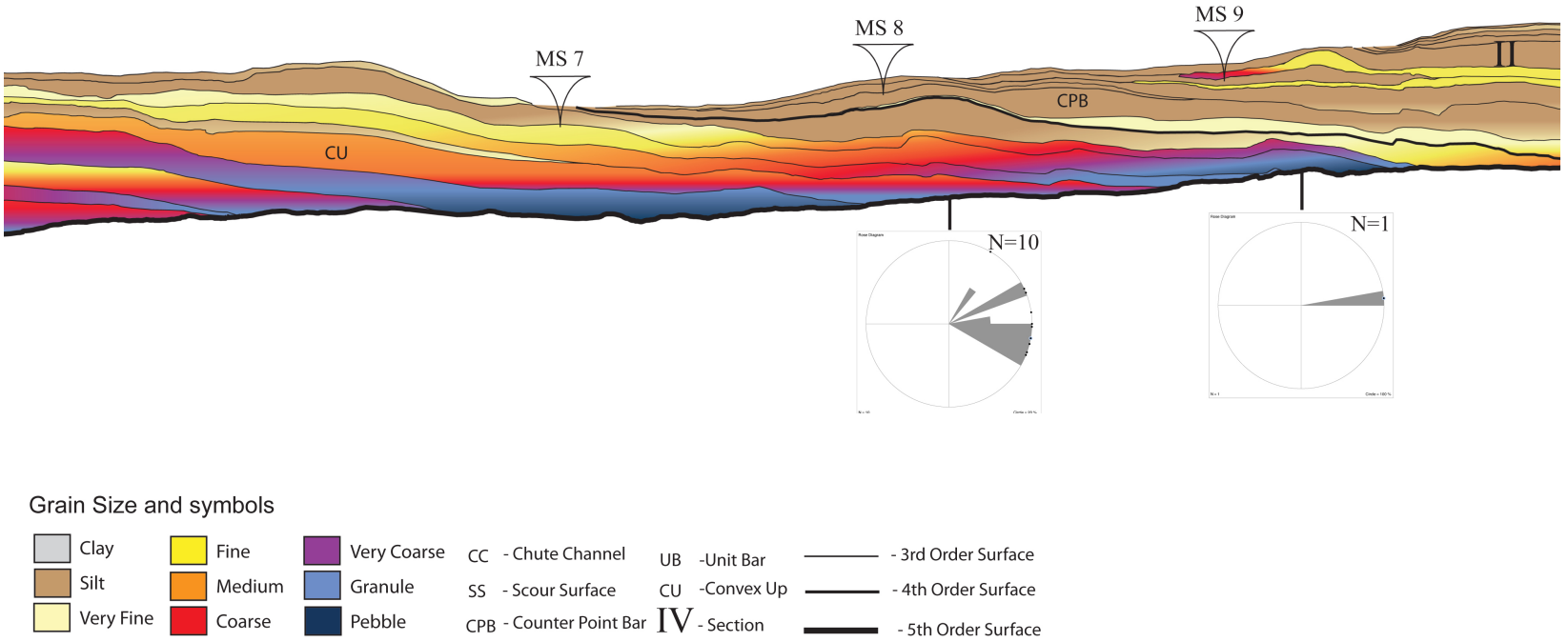

Figure 19. Bedding diagram of the central to eastern part of the outcrop. Notice paleocurrents going in an east to southeast direction, which together with the thickening of the finer grained deposits in the upper channel deposits could be a counter point bar.

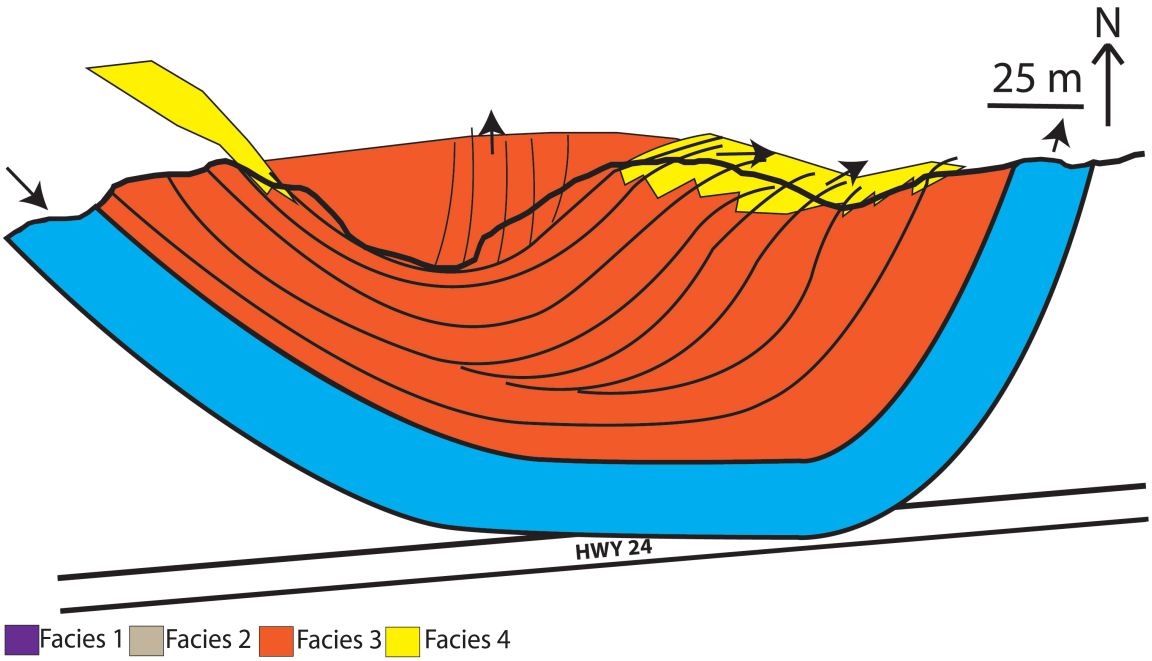

Figure 20. Shows channel reconstruction at latest time, where the paleocurrent measurements on the Eastern part of the outcrop are to north-northeast, while the flow in the western part of the channel is going to the southeast. Channel deposits are confirmed to be laterally limited to the west through trenching, while the deposits are inferred to be limited in lateral extent on the eastern margin of the outcrop from the presence of what could channel abandonement. At this time the deposits are showing the meanderloop to be expanding. Location of counter point bar deposits indicated by facies 4 (yellow), while active channel fill is by facies 3 (orange).

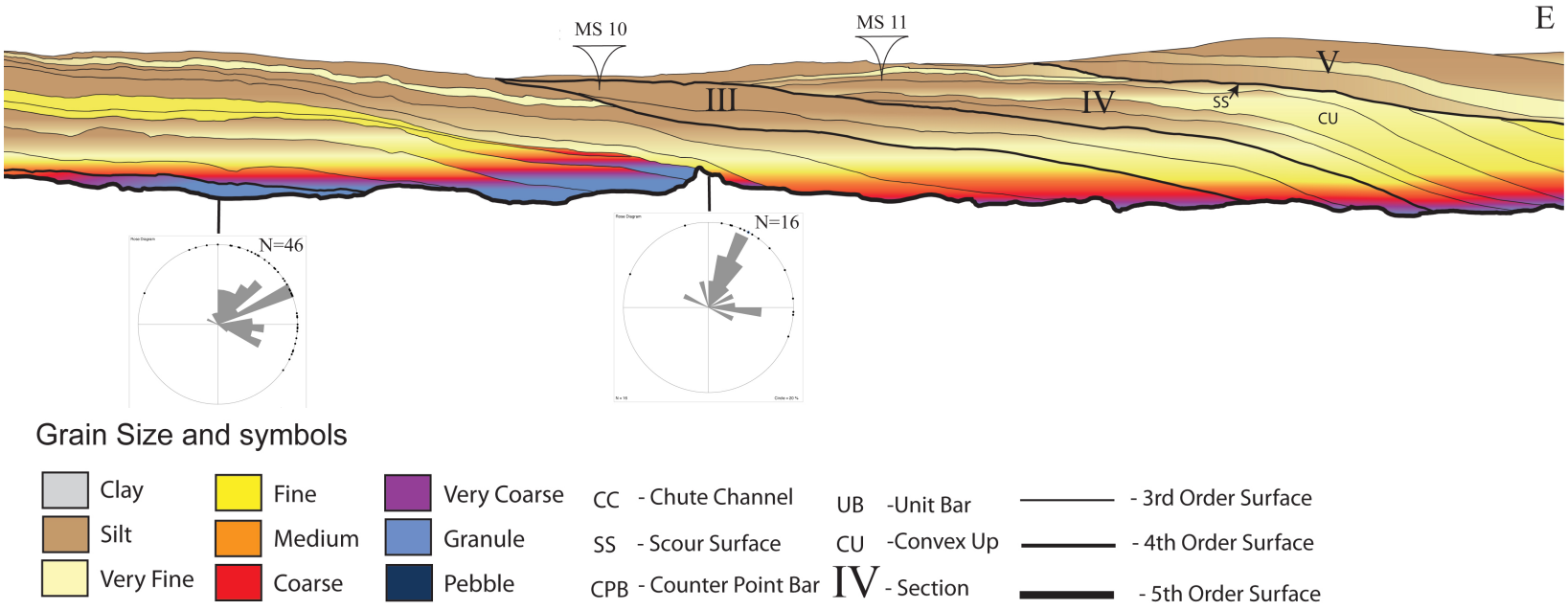

Figure 21. Bedding diagram with paleocurrents from the easternmost part of the outcrop showing a dominantly northeastern flow direction, and the bar accretion surfaces are dipping east.

Paleohydraulic Estimates

Various properties of the fluvial system were analyzed using calculations, including flow depth, channel width, discharge, and general flow direction. The channel width was determined from the length of accretionary surfaces, which averaged 23 meters, plus an estimate of the length of the cut bank at 7 meters. This was then corrected for the angle of flow compared to the angle of the outcrop by using a simple trigonometric function:

$$W_{true} = W_{app} * \sin(\theta_{out} - \theta_{flow})$$

Using the apparent measured width (W_{app}) of the channel at 30 meters with the average paleocurrent direction of flow (θ_{flow}) at 46 degrees and the angle of the outcrop (θ_{out}) at 333 degrees gave a true channel width (W_{true}) of 25.2 meters. Channel depth was calculated as an average of the heights of channel deposits of the 9 measured sections showing complete channel deposits, with extreme values of 4 meters at the shallowest, and 7 meters at the deepest end, with a mean of 5.6 meters, and the median being 5.8 meters.

Section	1	2	5	6	7	8	9	10	11
Depth	7m	6m	6.1m	6m	4m	5.4m	4.9m	4.9m	5.8m

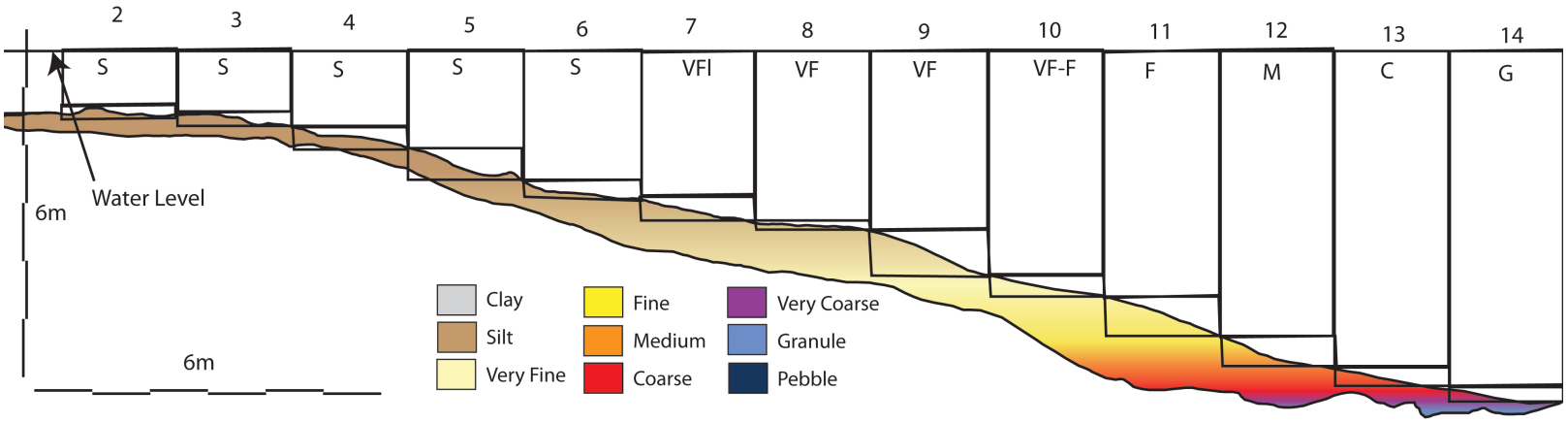

Figure 22. Diagram shows selected grain sizes across deposits thought to be part of the fluvial bedload, with each rectangle representing an area where discharge is to be calculated.

	1	**2**	**3**	**4**	**5**	**6**	**7**	**8**	**9**	**10**	**11**	**12**	**13**	**14**
Size	S	S	S	S	S	S	VFl	VF	VF	VF-F	F	M	C	G
Size (mm)	0.03	0.03	0.03	0.03	0.03	0.03	0.06	0.1	0.1	0.13	0.18	0.38	0.75	3
Area A(m^3)	0.9	1.9	2.1	2.5	3.3	4.4	4.9	5.6	6	7.5	8.3	9.8	10.7	11.3
Area B(m^3)	0	0.24	0.24	0.33	0.53	0.28	0.43	0.16	0.78	0.33	0.67	0.5	0.29	0.27
Area T(m^3)	0.9	2.1	2.3	2.8	3.8	4.7	5.3	5.8	6.8	7.8	9	10.3	11	11.6

Table 1. Table shows the grain size and area calculations forming the basis for further paleohydraulic calculations.

Each vertical section were covered by two rectangles, rectangle B with a corner through the lowest and highest part of the accretion surface, and rectangle A covering the entire water column from the top of B to the water surface. In order to calculate discharge, the area of each rectangle where there is water was calculated, for "A" type boxes it was a simply width multiplied by height, while for "B" boxes the calculated area was divided by two:

$$A_A = w * h_A$$

$$A_B = (w * h_B)/2$$

Values for critical bed shear stress was found in Fischenich (2001), and had been derived from two separate equations, one for gravel-sized sediments and one for sand sized sediments.

$$\tau_{cr} = (0.25 d_*^{(-0.6)}) * g(\rho_s - \rho_w) d * \tan\phi \text{ (sand)}$$

$$d^* = d((G-1)g/v^2)^{(1/3)}$$

$$\tau_{cr} = 0.06 * g(\rho_s - \rho_w) d * \tan\phi \text{ (gravel)}$$

This values for critical bed shear stress and critical shear velocity used were from table, and simply converted from ft/s to m/s through multiplication by 0.305. The τ_0 and u* values apply to non-cohesive equal-sized grains (Julien, 1995).

Class name	d_s (in)	ϕ (deg)	τ_{*c}	τ_{cr} (lb/sf)	V_{*c} (ft/s)
Boulder					
Very large	>80	42	0.054	37.4	4.36
Large	>40	42	0.054	18.7	3.08
Medium	>20	42	0.054	9.3	2.20
Small	>10	42	0.054	4.7	1.54
Cobble					
Large	>5	42	0.054	2.3	1.08
Small	>2.5	41	0.052	1.1	0.75
Gravel					
Very coarse	>1.3	40	0.050	0.54	0.52
Coarse	>0.6	38	0.047	0.25	0.36
Medium	>0.3	36	0.044	0.12	0.24
Fine	>0.16	35	0.042	0.06	0.17
Very fine	>0.08	33	0.039	0.03	0.12
Sands					
Very coarse	>0.04	32	0.029	0.01	0.070
Coarse	>0.02	31	0.033	0.006	0.055
Medium	>0.01	30	0.048	0.004	0.045
Fine	>0.005	30	0.072	0.003	0.040
Very fine	>0.003	30	0.109	0.002	0.035
Silts					
Coarse	>0.002	30	0.165	0.001	0.030
Medium	>0.001	30	0.25	0.001	0.025

Table 2. Shows τ_0 and u* for grain sizes varying from silt to boulders (from Julian, 1995).

	1 (S)	**2 (S)**	**3 (S)**	**4 (S)**	**5 (S)**	**6 (S)**	**7 (VF)**
u* (m/s)	0.009	0.009	0.009	0.009	0.009	0.009	0.011
	8 (VF)	**9 (VF)**	**10 (VF)**	**11 (F)**	**12 (M)**	**13 (C)**	**14 (G)**
u* (m/s)	0.011	0.011	0.011	0.012	0.014	0.017	0.037

Table 3. Shows values of u* converted to metric from the values of u* given by Julien (1995).

In order to use the 'Law of the Wall' with the u* values above, Y_0 (roughness height) was calculated for each column:

$$Y_0=D_{84}/30$$

The 'Law of the Wall' calculates flow velocity (u_y) at any flow depth (y). In order to get the average flow velocity of each rectangle, the following version of the law of the wall was used (Bridge, 2003):

$$u_y=u_*(1/k)*\ln(y/y_0)$$

$$U=1/(h-y_0)\ {}_{y0}\int^{h}\bar{u}(y)dy$$

$$U=(u^*/k)((\ln(h/y_0)-(1-(y_0/h))$$

	1	**2**	**3**	**4**	**5**	**6**	**7**	**8**	**9**	**10**	**11**	**12**	**13**	**14**
Size	S	S	S	S	S	S	VFl	VF	VF	VF-F	F	M	C	G
Size (mm)	0.03	0.03	0.03	0.03	0.03	0.03	0.06	0.1	0.1	0.13	0.18	0.38	0.75	3
Area A(m^3)	0.9	1.9	2.1	2.5	3.3	4.4	4.9	5.6	6	7.5	8.3	9.8	10.7	11.3
Area B(m^3)	0	0.24	0.24	0.33	0.53	0.28	0.43	0.16	0.78	0.33	0.67	0.5	0.29	0.27
Area T(m^3)	0.9	2.1	2.3	2.8	3.8	4.7	5.3	5.8	6.8	7.8	9	10.3	11	11.6
U (m/s)	0.3	0.3	0.3	0.3	0.3	0.3	0.3	0.3	0.3	0.3	0.4	0.4	0.5	0.9
Discharge (m^3/s)	0.3	0.6	0.7	0.8	1.1	1.4	1.8	1.9	2.2	2.6	3.3	4.1	5.1	10.4

Table 4. Values of area, average flow velocity (U) and discharge is shown in this diagram.

In order to calculate the total discharge of the fluvial system, the discharge values of 1-14 were added together, then the resulting sum was multiplied by 1.5 in order to account for all the water moving through the channel.

Total discharge:

$33\ m^3/s * 1.5 = 55 m^3/s$

Discussion

The outcrop shows bilateral downlap of accretion surfaces, with the eastern accretion units dipping east and the western accretion units dipping west. The paleocurrent measurements are generally southeast in the western part of the outcrop and northeast in the eastern part of the outcrop, and the measured sections show a fining upwards profile. All these indicators suggest that the studied outcrop is a fluvial deposit from a meandering river. The deposits are thought to represent a meaderloop that initially expanded (fig. 15), then translated eastwards (fig. 17) before going through a second expansion (fig. 20).

The bedding diagrams show several types of bar deposits, with unit bars of bar height less than water depth observed as the foundation of compound point bar deposits (figure 13 panel A). Point bar deposits make up the bulk of the channel deposits, and are characteristically dipping unidirectionally either eastward or westward. These point bar deposits are bounded by fourth order surfaces (fig 13 and 14), either obviously erosional in nature fig 14 panel E), others that merely have 3rd order surfaces onlapping and probably represent a shorter timespan of nondeposition. In the westernmost part of the diagram there is also an erosional surface truncating the top of a point bar deposit, interpreted as a chute channel that cut across the bar.

The fine-grained inclined beds within the deposits could either be counter point bar or flood drape deposits. The deposits are prevalent across the outcrop and are mainly found in the upper 1/3 of the of the channel deposits. The deposits most

likely to be CPBs are those where the fine-grained material is more concentrated and account for a higher percentage of the total channel thickness, such as between section 6 and section 8 (fig. 14, panels C and D) and those at section 2 (fig. 13 panel B) on the western side of the outcrop. A paleocurrent discrepancy at between section 7 and 8 (figure 14 panel D and figure 19) and a swell in the thickness of the fine-grained deposits both supports the idea that this could be a CPB. In addition, the paleogeographic reconstruction suggests the deposits to be concave in planview.

Lynds and Hajek (2006) describe five types of fine-grained deposits associated with braided fluvial deposits, as seen in figure 24.

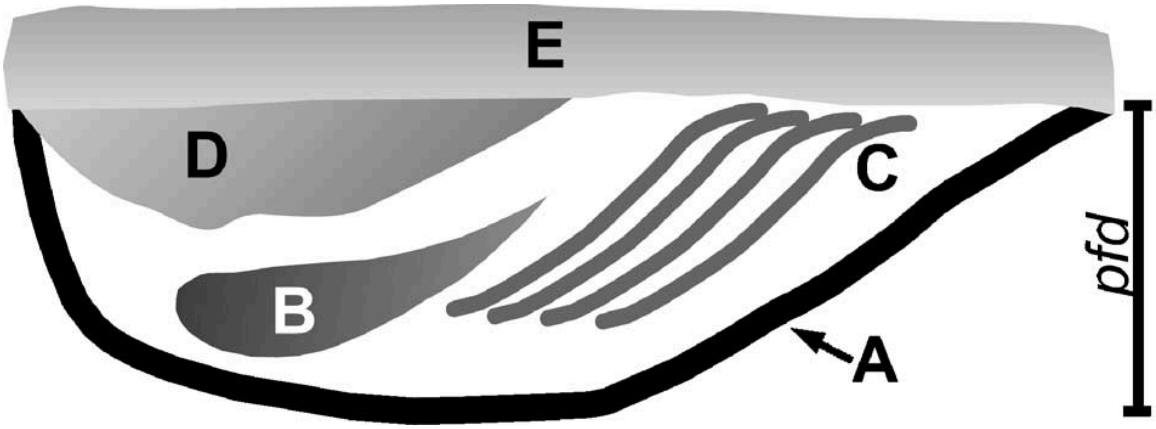

Figure 24. Diagram shows the five different types of fine-grained deposits found in braided fluvial deposits: A shows channel-lining muds, B shows interbar muds, C – inclined heterolithic strata, D – mud plugs, and E shows overbank/floodplain deposits (from Lynds and Hajek, 2006).

The five different kinds of heterogenic deposits described by Lynds and Hajek (2006) also apply to meandering fluvial deposits and are thought to each have distinct grain size distributions, as opposed to the two distinct grain size distributions of the fine-grained deposits observed in the studied outcrop. The deposits described in the Brushy Basin outcrop do not include any channel-lining nor any interbar muds. There is an abundance of IHS throughout the deposits however, as well as overbank/floodplain deposits.

Assessing paleohydraulics using the Law of the Wall has gives an opportunity to estimate flow velocity using simple equations, but the process is riddled with uncertainties. The sampling for the grain-size profile might be poor, in addition sampling of preserved deposits will be different from sampling of the transported bedload. One also supposes the roughness height of the deposits to be from planar beds, so it will not account for any differences in roughness height due to bedforms. Using any empirical equations to estimate bed shear stress is also a source of lessened accuracy as these are also limited to the conditions under which they were derived (Ro, 2007). Unlike using the Rubin and McCullogh (1980) bedform diagram, however, the Law of the Wall can be used to estimate the lesser flow velocities at shallower points of the river and thus will give a more nuanced picture of the total discharge.

The paleogeography of this area shows it being far from the coast (Dickinson and Gehrels 2009), and there is a complete absence of indicators of marine or tidal influence. Observing the outcrop exposure of the channel deposits, the coarser sandy channel

deposits are continuous, with the fine-grained upper point bar deposits mostly comprising 10-40% of total thickness, with a maximum of ~50% of total thickness. This should indicate that the entire sandstone body is continuous, as suggested in the "string of beads" model of Donselaar and Overeem (2008). This also conforms to the results of Willis and Tang (2010), which also showed meanderbelt deposits to develop laterally continuous sandstone units. This coarse-grained channelbelt with good interconnectivity should indicate the studied unit to have an excellent reservoir potential, however the heterolithic deposits making up the tops of the deposits will decrease permeability. The muddy floodplain deposits can also provide excellent reservoir seal pairs for these deposits.

Conclusions

The deposits represent a coarse-grained meandering fluvial channel flowing in an overall northeast direction. Reconstruction using bedding geometry and paleocurrent data shows the outcrop is the cross-section through deposits of a meanderloop going through expansion, then eastward translation, succeeded by additional expansion, with counter point bar deposits associated with the phase of eastward translation.

Facies analysis shows bentonite-rich siltstone interpreted to be floodbasin deposits along with thin elongate very fine- to fine-grained sandstone units showing soft-sediment deformation thought to be levee deposits. The lower channel deposits are coarse-grained with grain-sizes from pebble-size to fine sand, with the upper

part of the channel deposits showing silt to fine sand grain sizes. These fine-grained deposits are thought to be the counter point bar deposits.

Channel width is 25.2m with an average depth of 5.6m. Using the 'Law of the Wall', the highest average flow velocities were ~0.9 m^3/s, with the total discharge of the fluvial system being around 55 m^3/s.

References

Bridge, J. S., 2003, Rivers and Floodplains. Blackwell Publishing, 491 pp.

Campbell J. E., and Hendry, H. E., 1987, Anatomy of a gravelly meander lobe in the Saskatchewan River, near Nipawin, Canada. In: Recent Developments in Fluvial Sedimentology, SEPM Spec. Pub., v. 39, p. 179-189

Corbeanu, R. M., Wizevich, M. C., Bhattacharya, J. P., Zeng, X., McMechan, G. A., 2004, Three-dimensional architecture of ancient lower delta-plain point bars using ground-penetrating radar, Cretaceous Ferron Sandstone, Utah. AAPG Studies in Geology, v. 50, p. 427-449

Davidson, S. K., Hartley, A. J., 2010, Towards a quantitative method for estimating paleohydrology from clast size and comparison with modern rivers. Journal of Sedimentary Research, v. 80, p. 688-702

Dickinson, W. R. and Gehrels, G. E. , 2009, U-Pb ages of detrital zircons in Jurassic eolian and associated sandstones of the Colorado Plateau: Evidence for transcontinental dispersal and intraregional recycling of sediment. Geologic Society of America Bulletin, v. 121, p. 408-433

Donselaar, M. E., Overeen, I., 2008, Connectivity of fluvial point-bar deposits; an example from the Miocene Huesca fluvial fan, Ebro Basin, Spain. AAPG Bulletin, v. 92, p. 1109-1129

Fielding, C. R., Allen, J. P., Alexander, J., Gibling, M. R., Rygel, M. C., and Calder, J. H., 2011, Fluvial systems and their deposits in hot, seasonal semi-arid and sub-humid settings; modern and ancient examples. Special Publication – Society for Sedimentary Geology, May 2011, v. 97, p. 89-111

Fischenich, 2001, Stability thresholds for stream restoration materials. EMRRP Technical Notes Collection (ERDC TN-EMRRP-SR-29), U.S. Army Engineer Research and Development Center, Vicksburg, M.S., http://el.erdc.usace.army.mil/elpubs/pdf/sr29.pdf

Hickin, E. J., 1979, Concave-bank benches on the Squamish River, British Columbia. Canadian Journal of Earth Sciences, v. 16, p. 200-203

Hickin, E. J., 1986, Concave Bank benches in the floodplains of Muskwa and Fort Nelson rivers, British Columbia. Canadian Geographer, v. 30, p. 111-112

Julien, P. Y., 1995, Erosion and Sedimentation. Cambridge University Press, 280 pp.

Kostic, B., and Aigner, T., 2007, Sedimentary architecture and 3D ground-penetrating radar analysis of gravelly meandering river deposits (Neckar Valley, SW Germany). Sedimentology, v. 54, p. 789-808

Kowallis, B. J., Christiansen, E. H., Deino, A. L., 1991, Age of the Brushy Basin Member of the Morrison Formation, Colorado Plateau, western USA. Cretaceous Research, v. 12, p. 483-493.

Kowallis, B. J., Brooks, B. B., Greenhalgh, B. W., Sprinkel, D. A., 2007, New U/Pb zircon ages from an ash bed in the Brushy Basin Member of the Morrison Formation near Hanksville, Utah. Abstracts with Programs – Geological Society of America, v. 39, p. 9

Leclair, S. F., Bridge, J. S., 2001, Quantitative interpretation of sedimentary structures formed by river dunes. Journal of Sedimentary Research, v. 71, p. 713-716

Lynds, R., and Hajek, E. 2006, Conceptual model for predicting mudstone dimensions in sandy braided-river reservoirs. AAPG Bulletin, v. 90, p. 1273-1288

Makaske, B., Weert, H. J. T., 2005, Muddy lateral accretion and low-stream power in a sub-recent confined channel belt, Rhine-Meuse delta, central Netherlands. Sedimentology, v. 52, p. 651-668

McGowen, J. H., and Garner, L. E., 1970, Physiographic features and stratification types of coarse-grained point bars: Modern and ancient examples. Sedimentology, v. 14, p. 77-111

Miall, A. D., 1991, Hierarchies of architectural units in terrigenous clastic rocks, and their relationship to sedimentation rate. Concepts in Sedimentology and Paleontology, v. 3, p. 6-12

Ori, G. G., 1982, Braided to meandering channel patterns in humid-region alluvial fan deposits, River Reno, Po Plain (Northern Italy). Sedimentary Geology, v. 31, p. 231-548

Page, K. J. and Nanson, G. C., 1982, Concave-bank benches and associated floodplain formation. Earth Surface Processes and Landforms, v. 7, p. 529-543

Peakall, J., Ashworth, P. J., and Best, J. L., 2007, Meander-bend evolution, alluvial architecture, and the role of cohesion in sinuous river channels; a flume study. Journal of Sedimentary Research, v. 77, p. 197-212

Pyrce, R. S., Ashmore, P. E., 2005, Bedload path length and point bar development in gravel-bed river models. Sedimentology, v. 52, p. 839-857

Robinson, J. W., and McCabe, P. J., 1997, Sandstone-body and shale-body dimensions in a braided fluvial system; Salt Wash Sandstone Member (Morrison Formation), Garfield County, Utah. AAPG Bulletin, v. 81, p. 1267-1291

Ro, C., 2007, Principles of Fluvial Geomorphology. Routledge, 280 pp.

Roca, X., Nadon, G. C., 2007, Tectonic controls on the sequence stratigraphy of nonmarine retroarc foreland basin fills: Insights from the Upper Jurassic of central Utah. Journal of Sedimentary Research, v. 77, p. 239-255

Rubin, D.M., and McCulloch, D.S., 1980, Single and superimposed bedforms: A synthesis of San Francisco Bay and flume observations: Sedimentary Geology, v. 26, p. 207-231

Schumm, S. A., 1967, Meander length of alluvial rivers, v. 157, p. 1549-1550

Smith, S. A., 1987b, Gravel counterpoint bars: examples from the River Tywi, South Wales. In: Recent Developments in Fluvial Sedimentology, SEPM Spec. Publ., v. 39, p. 75-81

Smith, D. G., Hubbard, S. M., Leckie, D. A., Fustic, M., 2009, Counter point bar deposits; lithofacies and reservoir significance in the meandering modern Peace River and ancient McMurray Formation, Alberta, Canada. Sedimentology, v. 56, p. 1655-1669

Thomas, R. D., Smith, D. G., Wood, J. M., Visser, J., Calverly-Range, E. A., Koster, E. H., 1987, Inclined heterolithic stratification – terminology, description, interpretation and significance. Sedimentary Geology, v. 53, p. 123-179.

VanDeVelde, D. M., 2006, Paleosols as climate indicators of dinosaur sites, Brushy Basin Member of the Jurassic Morrison Formation, east-central Utah. Abstracts with Programs – Geological Society of America, v. 38, p. 63

Willis, B. J., Tang, H., 2010, Three-dimensional connectivity of point-bar deposits. Journal of Sedimentary Research, v. 80, p. 440-454

Willis, B. J., 1989, Palaeochannel reconstructions from point bar deposits: a three-dimensional perspective. Sedimentology, v. 36, p. 757-766

Woodyer K. D., 1975, Concave-bank benches on Barwon River, N.S.W. Australian Geographer, v. 13, p. 36-40